

OVERVIEW OF MITIGATION MODELS DEDICATED TO SEVERE ACCIDENTS AND CONSEQUENCES ON FLOW RATE THROUGH CONTAINMENT CONCRETE STRUCTURES

S. MIMOUNI*, P. BACONNIER[†] AND G. DAVY[‡]

*Electricite de France
Chatou, France
e-mail: stephane.mimouni@edf.fr

[†]Electricite de France
Chatou, France
e-mail: germain.davy@edf.fr

[‡]Ecole Superieure de Physique et Chimie
Paris, France
e-mail: paul.bacconnier@espci.fr

Key words: Cracks, two-phase flow, capillarity, condensation

Abstract. This study takes place within the framework of nuclear facilities containment assessment in the case of a hypothetical accident where a large amount of vapour is released. We propose in this paper to simulate the COPAIN test cases in order to assess the vapor condensation model implemented in our CFD tool. The importance of this model is twofold. Indeed, it is also essential to estimate the associated potential leakage rate, i.e. to assess the mass flowrate through cracks in the containment concrete structures. In this context, the vapor condensation along the walls in the cracks is of relevant interest.

INTRODUCTION

A severe accident in a PWR nuclear power plant generally originates from a lack of cooling of the core, whose residual power can no longer be evacuated. In a few hours, due to multiple failures, human or hardware, including the failure of backup procedures, the structure of fuel elements deteriorates. Hydrogen is produced from the oxidation of zirconium sheaths and of structures of fuel elements during the phase of core degradation. The hydrogen and water vapor thus produced are transferred to the containment and then transported by convection loops. Given the significant differences in density between hydrogen and other gases in the contain-

ment (nitrogen, oxygen, water vapor, carbon monoxide, carbon dioxide, ..), hydrogen can accumulate preferentially in the upper parts of the compartments of reactor building. In case of strong heterogeneity, hydrogen can achieve high local concentrations that exceed the threshold flammable gas mixture.

Among the different safety systems for limiting the pressure increase during the course of the accident and the impact of possible combustion (deflagration), French and German PWR reactors use two types of mitigation means.

1. The passive auto-catalytic recombiners (PAR): their role is to pro-actively oxidize hydrogen for preventing its accu-

mulation in the containment. The catalytic recombiners initiate a controlled combustion, which is similar to a slow deflagration.

2. Sprinkler systems: the injected water droplets cool the containment and lower the pressure by condensing steam on the droplets. They also promote mixing of gas by breaking quickly possible stratifications of the lightest gases.
3. The walls of the containment building and metal structures also play an important role from a thermal viewpoint. The walls, significantly cooler than the gas, condense the water vapor in the gas mixture and thus limit the pressure increase in the containment.
4. Furthermore, the temperature difference between fluid and walls generates convection loops, enhancing the mixing of gases having different density.

In order to understand with the hydrogen risk, our strategy was to increase gradually the level of complexity and to validate all the physical phenomena involved separately [Mimouni et al., 2017a]. As a consequence, dedicated models have been implemented in the CFD tool NEPTUNE_CFD by EDF in collaboration with CEA, FRAM-ATOME and IRSN. The first step is the analysis and the understanding of gas stratification and transport phenomena. In order to achieve this, CFD calculations are performed with two kinds of solver, namely NEPTUNE_CFD and *Code_Saturne*, for the PANDA test 17 [Mimouni et al., 2017a]. NEPTUNE_CFD is dedicated to the simulation of incompressible and compressible multi-component/multi-phase flows, whereas *Code_Saturne* is dedicated to homogeneous incompressible or low Mach number compressible flows, with only one momentum equation representing the mixture of gases,

liquid and particles. NEPTUNE_CFD is mainly used for nuclear engineering, whereas *Code_Saturne* is used for nuclear and fossil energy engineering, and for environment (as geophysical flows). NEPTUNE_CFD and *Code_Saturne* are the main solvers of the SALOME_CFD platform.

The vapor condensation along the wall of the containment building is the next step towards increasing complexity. The modelling proposed in NEPTUNE_CFD assumes that liquid droplets form along the wall. Vapor condensation on droplets makes them grow. Once the droplet diameter reaches a critical value, gravitational forces compensate surface tension force and then droplets slide over the wall. Droplets can also join the surrounding droplets and form a film layer [Mimouni et al., 2011a]. This modeling has been validated against the THAI-HR49 experiment, TOSQAN ISP-47 test [Mimouni et al., 2011a] and PANDA test 25 [Méchitoua et al., 2012].

The last step towards increasing complexity concerns the effects of spray modelling in the containment building. The two major thermal-hydraulic phenomena involved in spray behaviour in such applications are the thermodynamical effect of a spray (steam condensation on droplets and evaporation) and the dynamical effect (entrainment and mixing). But, steam condensation also leads to a local increase in the hydrogen concentration. Because of this local negative effect, dedicated CFD tools are required.

In the frame of the Severe Accident Research Network (SARNET), comparisons codes-experiments have been performed to evaluate the efficiency of these spray systems in terms of depressurization, hydrogen mixing and radioactive aerosols scavenging for applications concerned by nuclear reactor accidents. We briefly recall the main steps in the following.

Firstly, tests on a single falling droplet under typical gas conditions representative of a nuclear accident, have been proposed in the

frame of the SARNET2 network [Malet et al., 2014]. The drop diameter is modified by steam condensation or evaporation depending on the gas and droplet thermodynamical conditions (CARAIDAS experiment) [Mimouni et al., 2017a].

Secondly, two tests have been produced in the TOSQAN facility in order to study the spray behaviour under severe accident conditions: TOSQAN 101 and TOSQAN 113 [Mimouni et al., 2010]. The TOSQAN facility is a large enclosure (7 m³) devoted to simulate typical accidental thermal hydraulic flow conditions in nuclear-pressurized water reactor (PWR) containment.

A step further in the understanding of the phenomena involved in an industrial geometry can be achieved in the numerical simulation of two interconnected vessels, which is a main objective of this section. The two test cases analysed (namely ST30 and ST32) were conducted in the frame of the OECD/SETH2 project using the PANDA facility built at PSI (Switzerland) and have been calculated with NEPTUNE_CFD [Mimouni et al., 2017a]. These experiments of paramount importance provide valuable results into the formation of potentially dangerous hydrogen mixtures with increased hydrogen content in regions far away from the spray.

Moreover, a two-fluid multi-dimensional simulation with NEPTUNE_CFD, on the basis of two interacting real PWR spray nozzles, is compared to the results obtained on the CALIST facility. The influence of collisions between droplets is taken into account with a statistical approach based on the various outcomes of binary collisions [Mimouni et al., 2017a].

Finally, PAR modeling has been assessed with NEPTUNE_CFD in [Mimouni et al., 2011b]. The sensitivity to the mesh refinement has been extensively verified in all test cases and results can be found in [Mimouni et al., 2017a].

Moreover, integrity tests are realized every 10 years to check the effective ability of the containment building in complying with regulations. During these tests, the gas mass flowrate through the containment concrete structures is measured. Considering there is no steel liner on the internal vessel and only concrete has to provide the air tightness, it is essential to estimate the associated potential leakage rate. In the case of a hypothetical accident where a large amount of vapour is released, an air-vapor mixture infiltrates into cracks. Firstly, vapor condensates onto the walls inside the crack. Thin droplets coalesce which leads to the formation of a continuous liquid field, called capillary bridge [Washburn, 1921]- [Persoff et al., 1995]- [Turner et al., 2004]. The presence of capillary bridges is of relevant interest and could drastically decrease the gas flow rate through containment structures, which could be highly favourable to safety. But, very few CFD studies have been reported in the literature except [Rastiello et al., 2015].

The objective of this paper is to underline for the first time the key role of the phenomenon of vapor condensation both for the hydrogen risk and for the assessment of the mass flowrate through cracks in the containment concrete structures. As a consequence, we propose in the paper an assessment of the wall condensation model. In a second stage, we give a physical analysis of the vapor condensation in a crack in order to establish the main requirements for future experiments and simulations.

1 MATHEMATICAL AND NUMERICAL CONCEPTS

The solver, based on a pressure correction approach, is able to simulate multi-component multiphase flows by solving a set of three balance equations for each field (fluid component and/or phase) [Ishii, 1975]. These fields can represent many kinds of multiphase flows: distinct physical components (e.g. gas, liquid and solid particles); ther-

modynamic phases of the same component (e.g.: liquid water and its vapor); distinct physical components, some of which split into different groups (e.g.: vapor and several groups of different diameter droplets); different forms of the same physical components (e.g.: a continuous liquid field, a dispersed liquid field, a continuous vapor field, a dispersed vapor field). The solver is implemented in the NEPTUNE software environment, which is based on a finite volume discretization, together with a collocated arrangement for all variables. The data structure is totally face-based which allows the use of arbitrary shaped cells (tetrahedra, hexahedra, prisms, pyramids ...). NEPTUNE_CFD and *Code_Saturne* share numerical solvers and pre/pro postprocessing tools. Both CFD codes are encapsulated in the SALOME_CFD platform.

1.1 Standard equations solved by NEPTUNE_CFD

Flows in NEPTUNE_CFD are modeled with a Eulerian description, using the two-fluid model of Ishii extended to n-field [Ishii, 1975]. This model is composed of three main equations: the mass balance equation, the momentum balance equation and the energy balance equation. These equations are solved for each field and for each time step.

1.1.1 Mass Balance Equation

$$\frac{\partial \alpha_k \rho_k}{\partial t} + \vec{\nabla} \cdot (\alpha_k \rho_k \vec{u}_k) = \Gamma_k \quad (1)$$

Where:

- k is the considered field
- α_k is the volume fraction of field k
- ρ_k is the density of field k
- \vec{u}_k is the velocity of field k
- Γ_k is the mass transfer between the field k and all the other fields

In particular, in the case of phase change, the mass transfer from the field j to the field k is:

$$\Gamma_{j \rightarrow k} = \frac{Q_{j \rightarrow k} + Q_{k \rightarrow j}}{H_j - H_k} \quad (2)$$

Where:

- $Q_{j \rightarrow k}$ is the heat transfer from field j to field k
- H_k is the enthalpy of field k

1.1.2 Momentum Balance Equation

$$\frac{\partial \alpha_k \rho_k \vec{u}_k}{\partial t} + (\alpha_k \rho_k \vec{u}_k \cdot \vec{\nabla}) \vec{u}_k = \quad (3)$$

$$\vec{\nabla} \cdot (\alpha_k \eta_k \vec{\bar{S}}_k) - \alpha_k \vec{\nabla} P + \alpha_k \rho_k \vec{g} + \vec{F}_{i_k} \quad (4)$$

Where:

- \vec{g} is the gravity acceleration
- F_{i_k} is the interfacial momentum transfer associated with field k .
- $\vec{\bar{S}}$ is the viscous stress tensor with:

$$S_{ij} = \frac{\partial u_i}{\partial x_j} + \frac{\partial u_j}{\partial x_i} - \frac{2}{3} \frac{\partial u_i}{\partial x_i} \delta_{ij} \quad (5)$$

1.1.3 Energy Balance Equation

$$\frac{\partial \rho_k H_k}{\partial t} + \vec{\nabla} \cdot (\rho_k H_k \vec{u}_k) = \quad (6)$$

$$-\vec{\nabla} \cdot \vec{Q} + \vec{\nabla} \cdot (\eta_k \vec{\bar{S}}_k \cdot \vec{u}_k) + \rho_k \vec{g} \cdot \vec{u}_k + \quad (7)$$

$$\frac{\partial P}{\partial t} + \vec{\nabla} P \cdot \vec{u} \quad (8)$$

Where:

- $\vec{Q}_k = -\lambda_k \vec{\nabla} T_k$ is the interfacial heat flux associated with field k

- λ_k is the thermal conductivity of field k
- T_k is the temperature of field k
- H_k is the total enthalpy of field k defined as:

$$H_k = e_k + \frac{1}{2}u_k^2 + \frac{P}{\rho_k} \quad (9)$$

Where e_k is the intern energy of field k .

2 COPAIN TEST CASES

2.1 Physical models

The main phenomenon simulated in this section is the vapor condensation at the wall in presence of non condensable gases with a two-phase flow approach. As a consequence, we solve mass, momentum and energy balances for both gas phase and liquid phase (droplets). In this section, the gas phase is a mixture of vapor and air. Thus, we solve a supplementary equation for the mass conservation of the air mass fraction. The standard turbulence model in NEPTUNE_CFD is the $R_{ij}-\epsilon$ model but, for the hydrogen risk topic (studies in the containment geometry), the turbulence effects are modelled with the $K-\epsilon$ model (see details in [Mimouni et al., 2017a]). Indeed, $R_{ij}-\epsilon$ model needs a mesh refinement not compatible with the simulation of whole containment. The only force exerted on droplets are the drag force. Heat and mass transfers dedicated to the vapor condensation are detailed in [Mimouni et al., 2011a]. The main dimensionless numbers are the Nusselt number (dimensionless thermal heat flux) and the Sherwood number (dimensionless mass transfer). In this section, we keep an monodispersed approach and we neglect the coalescence and break-up phenomena for the droplets: the droplet diameter evolves because of mass transfer with the gas phase. So, we solve a supplementary equation to take into account the droplet diameter variations.

2.2 Case description

The COPAIN facility (Bazin, 1999) deals with studying the phenomenon of wall condensation in the presence of non-condensable gases. The experimental section is composed by a rectangular channel that is placed vertically and with a width and depth dimension of 0.6 m and 0.5 m respectively. The condensation plate is 2 m long and 0.6 m wide.

The computational domain is half of the physical domain (symmetry). The sensitivity to the mesh refinement have been assessed and proved to be acceptable. The grids are uniform, including the nearest cells to the wall. Results are similar between “standard” and fine mesh with the two-phase flow approach developed in the paper. The condensation flux is measured along the cold wall (vertical axis in figure 1) and compared with calculations (figures 2 to 6).

Table 1: Boundary conditions
V: gas velocity (m/s), P: pressure (bar), Tg: gas temperature (K), Tw: wall temperature (K), Air: air mass fraction, He: helium mass fraction

Test	V	P	Tg	Tw	Air	He
P344	0.3	1.21	344.03	322.00	0.8640	0.0000
P441	3	1.02	353.23	307.40	0.7670	0.0000
P443	1	1.02	352.33	300.06	0.7720	0.0000
P444	0.5	1.02	351.53	299.70	0.7730	0.0000
P461	3	1.22	344.43	329.92	0.7354	0.0676

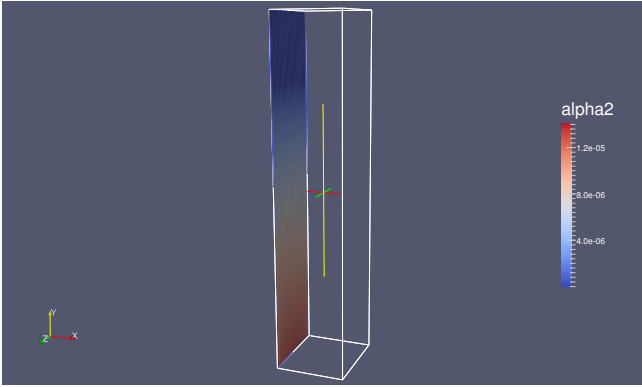


Figure 1: COPAIN test case. Visualization of the liquid fraction along the cold wall and created by condensation.

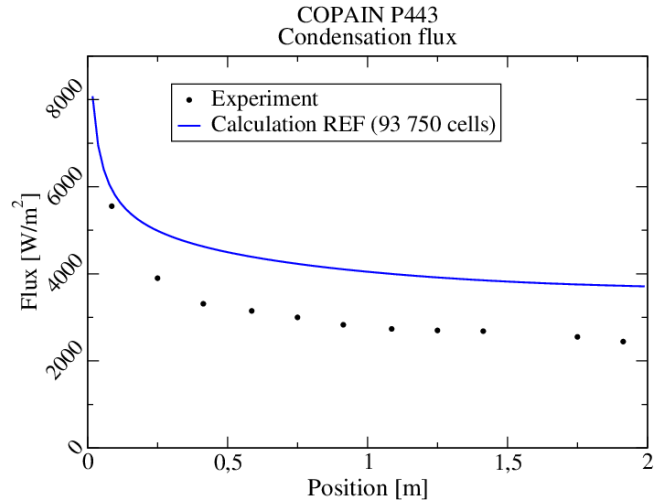


Figure 4

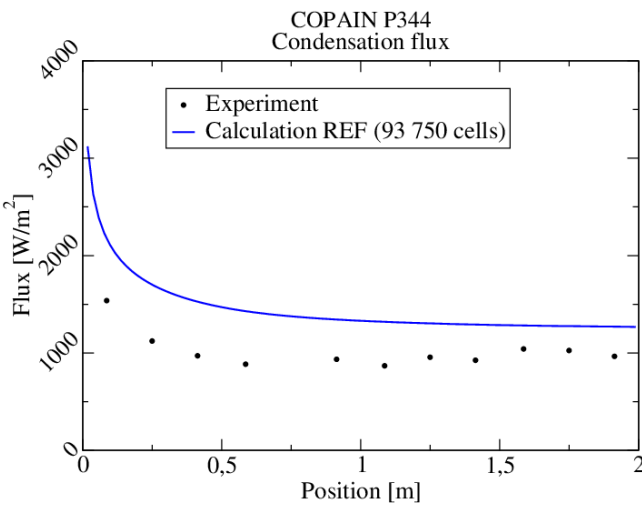


Figure 2

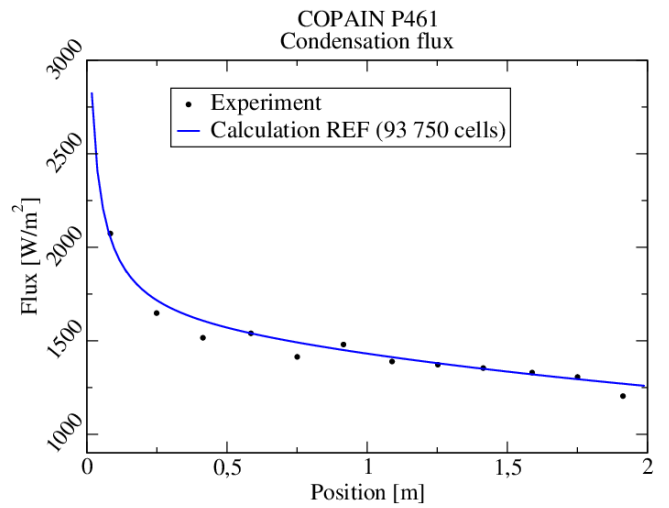


Figure 5

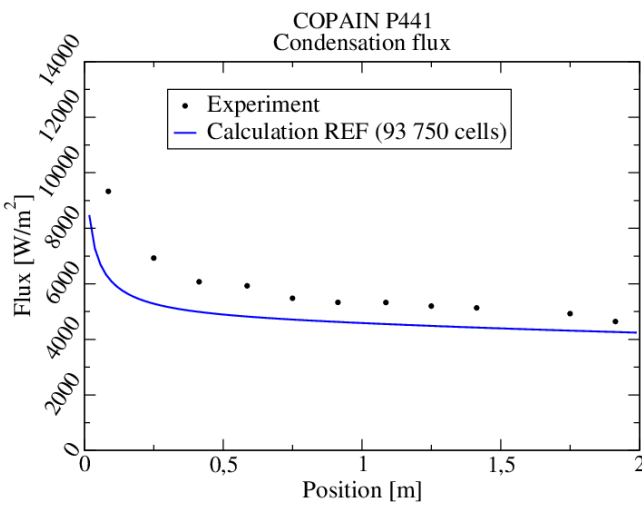


Figure 3

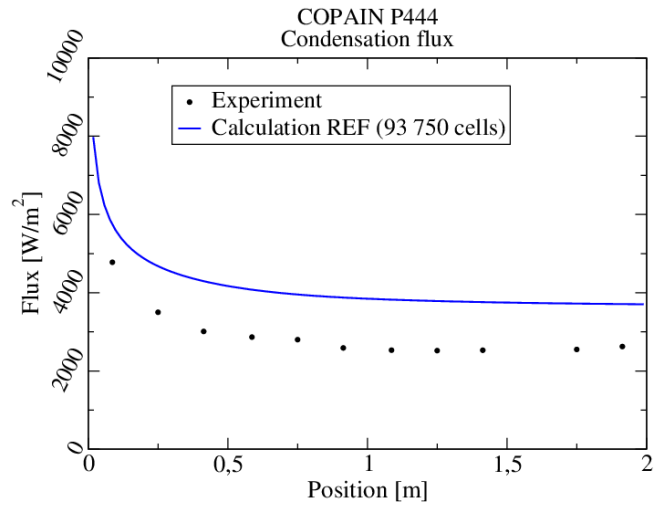


Figure 6

Figures 2 to 6 show that calculations and experimental data are in reasonable agreement.

3 MULTIFIELD APPROACH FOR TWO-PHASE FLOWS : APPLICATION TO TWO-PHASE FLOWS THROUGH A CRACK

This approach is based on the two-fluid model with an Eulerian description of the small spherical inclusions extended to n-phases or n-fields: mass, momentum and energy balances are solved for droplets, continuous liquid field and continuous gas field. The large deformable structures are simulated by considering them as junctions between two continuous fields. Large interfaces are calculated by an interface tracking method [Bonometti and Magnaudet, 2006]. The simulation of the small spherical inclusions in a carrier field has been widely validated but the large interfaces remain challenging. A model dedicated to the simulation of large interfaces has been implemented in the CFD tool. It is composed by a surface tension model [Coquerelle and Glockner, 2015]- [Brackbill et al., 1992]- [Renardy and Renardy, 2002]- [Francois et al., 2006]- [Popinet and Zaleski, 1999], a drag force law necessary to couple the velocity of the two continuous fields at the interface and an interface sharpening equation. This last element is crucial since the two-fluid model diffuses artificially large interfaces. However, the introduction of this equation in the NEPTUNE.CFD code requires paying attention to mass conservation and spurious velocities which has been carried out by a special numerical treatment. Details can be found in [Fleau, 2017]- [Mimouni et al., 2017b]- [Vincent et al., 2016].

Finally, the three-field approach can be seen as a generalization of the standard two-field approach.

The approach presented above, can be applied in the understanding of many situations occurring in nuclear power plants as the CFD

modeling of the flow rate through containment concrete structures by a multifield approach as explained on below.

We remind that this study takes place within the framework of nuclear facilities containment assessment in the case of a hypothetical accident where a large amount of vapour is released. An air-vapor mixture infiltrate into cracks. Firstly, vapor condensates onto the walls inside the crack. Thin droplets coalesce which leads to the formation of a continuous liquid field. The presence of capillary bridges is of relevant interest and could drastically decrease the gas flow rate through containment structures, which could be highly favourable to safety. We underline that, at this stage, we do not take into account the liquid film created by the vapor condensation along the containment walls. It seems clear, that this amount of liquid at the inlet of the crack is favourable to safety. From a conservative point of view, we neglect it in the following. Moreover, further into the crack, the flow could be very complex: it is constituted of small droplets and small bubbles into the continuous liquid phase. The presence of four phases makes the numerical simulation much more difficult to achieve because mass and heat transfers take place between each field with all the others.

We model separately the droplets and the capillary bridges. The simulation consists in treating the droplets as a dispersed field and locating the interface of capillary bridges. The main phenomena are:

1. the vapor condensation in presence of non condensable gases onto the walls of the crack and along the liquid film;
2. the mass transfer between the dispersed field (droplets) and the continuous liquid field;
3. the capillarity effect which plays the main role at the crack scale.

The modeling of these phenomena is currently under development in the CFD tool

NEPTUNE_CFD.

The main point is the modelling and the validation of the capillary model implemented in the CFD tool. The modeling of capillary effects has been validated against two cases (not presented in the paper):

1. the verification of the Jurin's law which describes the rise and fall of a liquid in a capillary tube;
2. the simulation of a water drop impacting a hydrophilic surface (wetting) or a hydrophobic surface (non-wetting) [Guillaument et al., 2014]- [Wang et al., 2014]- [Fujimoto et al., 2007]- [Qu  r  , 1997];

Moreover, these simulations highlight the propagation of spurious currents. They have been measured in [Fleau, 2017], where it is proved that the mesh refinement decreases their level (the model implemented converges). We investigate in the following section pros and cons of such a calculation strategy.

3.1 Spatial dilatation

The bone of contention of the numerical simulation of submillimetric cracks is that the volume of each cell becomes very small when one refines the mesh. Indeed, we are talking about really small lengths scale compared to usual NEPTUNE_CFD applications. This issue is directly linked to the time step necessary to perform the simulation which can decrease until reaching $10^{-6} - 10^{-7} s$ which is the common limit of the time step with NEPTUNE_CFD. The idea that one can have is to dilate the size of the computational domain and to adapt physical quantities, such as the surface tension coefficient σ , or the viscosity η in order to conserve some dimensionless numbers describing the flow. The first step is then to determine these important dimensionless numbers, and then to establish what modifications have to be applied to the physical quantities of the

flow when one dilates the size of the domain by a factor k .

3.2 Main dimensionless numbers

The dimensionless numbers of interest regarding thin films and capillary phenomenon inside a submillimetric crack are the following:

$$\text{Capillary number } Ca = \frac{v\eta}{\sigma} \quad (10)$$

$$\text{Deryagin number } De = \frac{L}{\kappa^{-1}} \quad (11)$$

$$\text{Weber number } We = \frac{\rho v^2 L}{\sigma} \quad (12)$$

$$\text{Reynolds number } Re = \frac{vL}{\nu} \quad (13)$$

Ca represents the relative effect of viscous forces versus surface tension. We measure the relative importance of the fluid's inertia compared to surface tension. Re is the ratio of inertial forces to viscous forces. Finally, De represents the ratio between the characteristic size of a film and the capillary length. The conservation of this number means to dilate the capillary length and the size of the domain by the same factor.

3.3 Scaling relations

All the relations we will derive will depend on the spatial dilatation. Let's note L' the size of the domain after the dilatation: $L' = kL$, with k the scaling factor. Moreover, we need to define what are the variables of the problem. The local velocity v can not be one of them because all the previous relations deals with local velocity. Change the global flow rate will not allow conserving locally all the 4 dimensionless numbers before and after the spatial dilatation. That means $v_g = v'_g$ and $v_w = v'_w$, where the index g stands for gas (mixture of air and vapor) and the index w stands for water. Thus, the variables are the characteristics of the fluids:

- For the water η_w , and ρ_w .
- For the air η_g , and ρ_g .
- The surface tension coefficient σ_{wa} , called simply σ .

This choice of variables will allow us to find a “simulating fluid” which will flow in the same manner in a dilate domain than the water in the original domain. As a consequence, it could have experimental outcomes. This point is of paramount importance: the thickness of the wall for the containment is about 120 cm but less than 50 cm in most of experiments. If initial thermohydraulics conditions typical of severe accident are applied to an experiment designed to study a two-phase flow through a crack, then it is clear, for example, that the pressure gradient across the crack is not representative of the real situation studied. Obviously, only dimensionless numbers must be conserved between the real situation and the experimental setup.

We consider only the water because the reasoning remains still valid for gas. Solve the problem means to find η'_w , ρ'_w and σ' by equalizing the 4 dimensionless numbers.

Moreover, we have to conserve another dimensionless number representing the pressure difference between the two extremities of the channel (crack); for this we consider the Bejan number Be which is the analog of the Laplace number $La = \frac{Re^2}{We}$ (dimensionless ratio of the surface forces over the inertia and the viscous forces), which can be seen as a dimensionless pressure difference:

$$Be = \frac{\rho \Delta P L^2}{\eta^2} \quad (14)$$

To sum up, the scaling relations for the properties of the fluids (gas and liquid) and the pressure gradient are:

$$\frac{\eta'_w}{\eta_w} = \frac{\sigma'}{\sigma} \quad (15)$$

$$\frac{\eta'_g}{\eta_g} = \frac{\sigma'}{\sigma} \quad (16)$$

$$\frac{\rho'_w}{\rho_w} = \frac{1}{k} \frac{\sigma'}{\sigma} \quad (17)$$

$$\frac{\rho'_g}{\rho_g} = \frac{1}{k} \frac{\sigma'}{\sigma} \quad (18)$$

$$\frac{\nabla P'}{\nabla P} = \frac{1}{k^2} \frac{\sigma'}{\sigma} \quad (19)$$

With the given ratio σ'/σ , the simulating fluids that can be used to describe exactly a situation after the scaling takes place on a hypersurface described by the set of physical properties. Experimenters could use this hypersurface to choose a real fluid and study microscopic phenomena that occur in a crack. The conservation of the Deryagin number is ensured by the calculation of $\frac{g'}{g}$.

4 Narrowing study

4.1 Model description

The incompressible two-phase (water + air) flow through a single horizontal rectangular channel (with high length-to-height ratio) comprising a convergent-divergent duct is numerically simulated. The initial condition is represented in figure 7 by a symmetric convergent-divergent duct. The air and the water are initialized at rest. The water takes place in the form of a drop at a distance d from the beginning of the crack. All the simulations will be done in a 2D cartesian mesh.

We initialize a single circular drop of water, $R = 0.5H$ in radius, at a distance d from the beginning of the crack. When the water touches the solid wall, it is compressed and form a bridge. Depending on the water wettability, i.e. θ_E , concave-concave or convex-convex tail (rear) and nose (front) interfaces form. The initial situation is the dynamic equilibrium, as in pressure than in contact angle. We do not take into account

the capillary effect (in this study) in order to reduce the spurious velocities. The static contact angle is therefore 90° , as in standard NEPTUNE_CFD. In future calculations, the capillary models will be used in order to impose a contact angle more realistic.

In a first stage, the drop reaches a mechanical equilibrium. In a second stage, calculations are performed by imposing a pressure difference $\Delta P = P_{in} - P_{out}$ between the inlet ($x = 0$) and outlet ($x = L$) sections of the channel to see if the water drop is expelled or not. A no-slip condition is used to state that, at a solid boundary, the relative fluid velocity with respect to the channel wall is null.

In this section, we apply the scaling relations established previously. We simulate a crack of diameter 1mm and we take $k = 10$ and $\gamma'/\gamma = 1$.

Before discussing the details of particular properties of the flow evolutions, it is worth noting that strong flow rate fluctuations are observed when the water drop passes through the convergent-divergent duct. In this phase, due to the applied pressure gradient and viscous interactions with the solid walls, the water menisci's curvatures evolve. The resulting capillary pressure induces flow accelerations/decelerations (i.e. the average Reynolds number increases/decreases). Furthermore, under particular geometrical and kinematic conditions, the flow rate can decrease down to zero even if a nonzero pressure difference is imposed between the channel extremities (i.e. the water drop acts as a cork). The quantification of the different interactions is not easy because the water drop deformations are strongly influenced by the coupled effect of the contact angle, the orientation of the solid walls, and the pressure gradient. This latter aspect is important, as the flow can induce a strong asymmetrical deformation between nose (front) and tail (rear)

fluid-fluid interfaces, even in absence of geometrical irregularities.

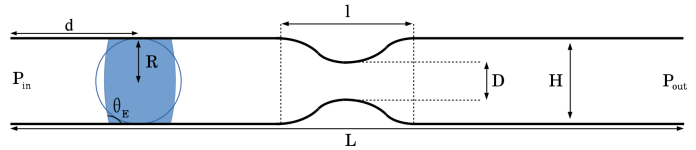


Figure 7: Geometry of the channel definition and illustration of the initialization of the water drop. The narrowing has a sinusoidal shape.

4.2 Blocking condition

As we will see in the next section dedicated to the results of the previous model, the drop can stop the flow when it arrives into the narrowing. This is due to another pressure gradient which balances the external pressure gradient. To understand why we have to remind the Laplace law describing the pressure jump at an interface for a constant curvature:

$$\Delta P = \gamma \kappa \quad (20)$$

with κ the curvature of the considered interface. Moreover, the drop inside the narrowing has two interfaces, as one can see in figure 7, and each of them if submitted to the Laplace law. The upstream menisci will be characterized by the subscript “t” for tail, and the downstream menisci by the subscript “n” for nose. If we assume that the interfaces are at a distance a , the pressure gradient into the drop induced by the curvature is:

$$\nabla P_\kappa = -\gamma \frac{\kappa_n + \kappa_t}{a} \quad (21)$$

As a consequence, the drop is at the mechanical equilibrium only if:

$$\nabla P_\kappa = \gamma \frac{\kappa_t + \kappa_n}{a} = \gamma \frac{\Delta \kappa}{a} = \nabla P_{channel} \quad (22)$$

with $\Delta \kappa$ a quantity which depends on the geometry of the problem ($h(x)$, D/H , ...), on the physical properties of the fluids (θ_E , γ ,

...), on the external pressure gradient between the crack's extremities $\nabla P_{channel}$, and on the position of the drop in the crack. This relation is then highly non-linear and dependent on various parameters. As long as this relation is satisfied, the drop can be at the mechanical equilibrium. But for high-pressure gradients, the interface can not deform as much as it should in order to balance the pressure difference. This point underlines the existence of a critical pressure gradient after which the drop will not be able to stop.

4.3 Fixed Bejan number

The figure 8 represents the time evolution of the Reynolds number for the finest grid (200x2000) used in this study. The figure presents the flow rate evolution when the drop passes through the convergent-divergent. Time evolutions of nose and tail interface curvatures κ_n and κ_t are represented too, in order to better understand fluid dynamics and confinement effects. Curvatures of the interfaces are computed everywhere in the domain but we use the curvature in the line defined by the middle of the domain in the directions orthogonal to the direction of the crack, and we evaluated them at the maximum of the field $\alpha_1\alpha_2$ on this line. Numerical results show that flow rate fluctuations strongly depends on the water drop interface positions within the convergent-divergent duct. The average Reynolds number inside the drop evolves schematically according to the following main phases:

- **Phase 1:** Before the drop reaches the convergent duct, the mass flow rate remains constant and equal to its initial value ($Re = Re_{eq}$). In this phase, a negative capillary pressure difference between both menisci results from the asymmetric menisci's curvature. Nose curvature induces an enhancement in flow intensity, while the tail has the opposite effect. The resulting effect is opposite to the external pressure gradient

(i.e. it tends to decelerate the flow).

- **Phase 2:** When the nose interface is within the entrance, there is a coupling between the reduction of the channel section, which tends to accelerate the flow, and the increasing of the negative capillary pressure, which decelerate the flow. As a consequence, the flow decelerates during this phase. This is the balance between the two previous effects that is responsible for the observed non-linear $Re(t)$ evolution.
- **Phase 3:** Once the front interface passes through the diverging zone, nose curvature decreases (in absolute value), and tail curvature too, up to inverse its convexity. During this phase, the resulting capillary pressure is close to zero and increases. This force balances with the presence of the convergent-divergent, and as a result the average flow rate begins constant and increase swiftly.
- **Phase 4:** The inversion of the tail curvature leads to a strong positive capillary pressure. This effect should increase the flow rate but as the drop begin to enter the divergent part, the resulting is a slow enhancement of the flow rate.
- **Phase 5:** When the tail passes the middle of the narrowing, the curvature recover its initial sign and increase drastically. It results a strong negative capillary pressure and as the divergent duct have the same effect, the resulting flow rate continues to decrease down to its minimum value ($Re = Re_{min}$). As a consequence, if the drop stops into the narrowing, it can only be when it passes through the divergent part which will be the equilibrium position. Then, the more the drop advances in the divergent duct, the more the tail

curvature approaches its initial value. It results that the capillary pressure decreases (in absolute value) and as a consequence, the flow rate increases.

- **Phase 6:** When the drop is again within the parallel-plates zone, the initial Reynolds value is recovered progressively ($Re \rightarrow Re_{eq}$)

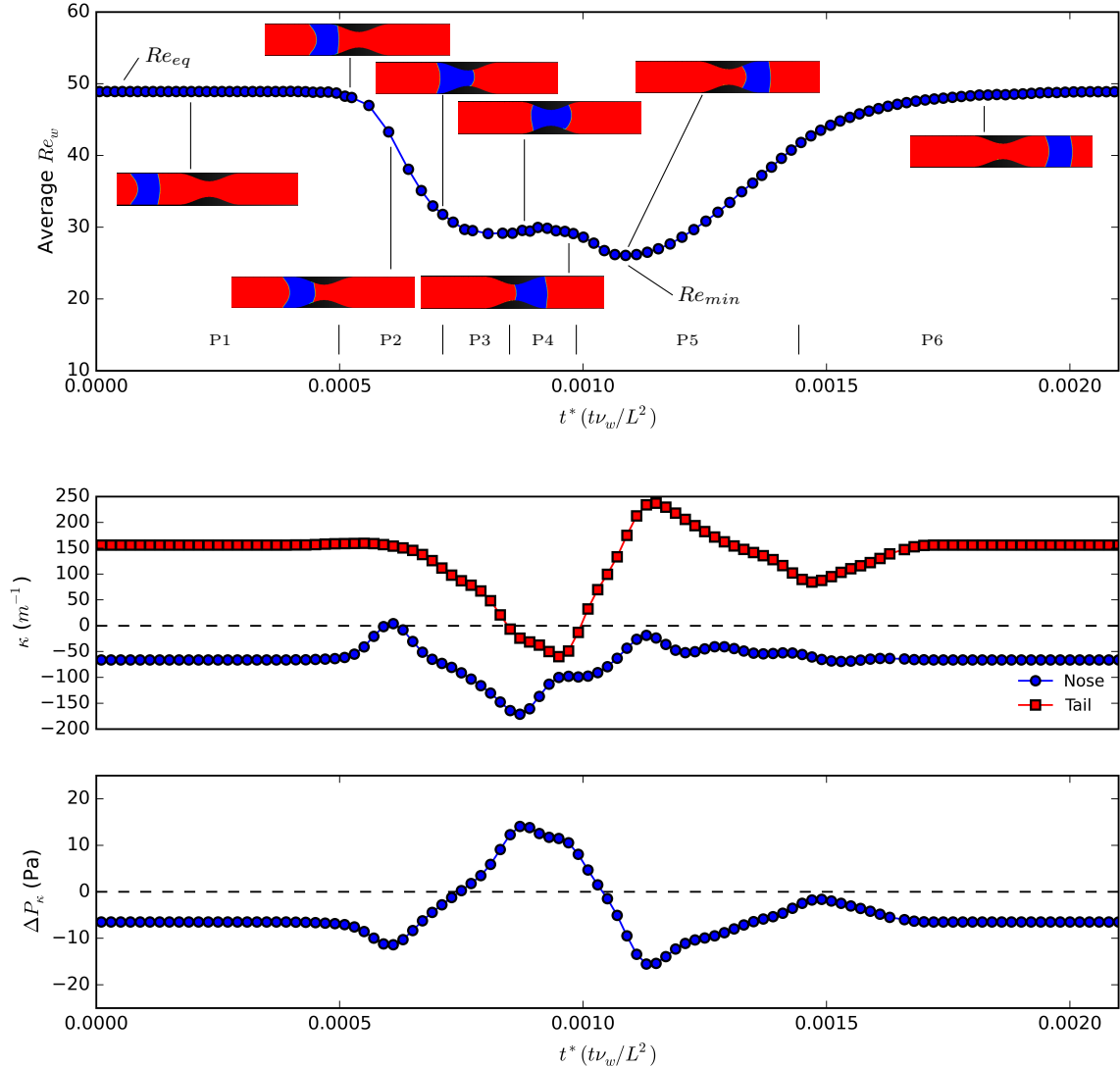


Figure 8: (top) Average Reynold number of the drop according to the dimensionless time (middle) Drop rear (tail) and front (nose) interface curvature according to the dimensionless time (bottom) Pressure difference induced by the curvature differences. ($\nabla P = 2.10^4 Pa/m$, $Be = 2.10^5$, $D/H = 0.5$, $\theta_E = 90^\circ$)

CONCLUSION

Gas stratification and vapour condensation at the walls in the containment building have been assessed in previous studies [Mimouni et al., 2017a]. In the paper, we

present the validation of the COPAIN test cases. Calculations compare reasonably well with experimental data and give an idea of the degree of maturity of CFD codes used at EDF for severe accident H2 risk assess-

ment. The importance of vapor condensation is twofold.

Indeed, in the case of a hypothetical accident where a large amount of vapour is released, an air-vapor mixture infiltrate into cracks. The simulation of such a flow needs a multifield approach where interfaces between continuous gas field and continuous liquid field are calculated by an interface tracking method. Supplementary models as surface tension force, generalized drag force and capillarity are taken into account (details can be found in [Fleau, 2017]- [Mimouni et al., 2017b]).

In this context, we derived 5 scaling relations which allow conserving the dimensionless numbers characteristic of the flow when one can neglect the gravity. These relations allow performing simulations with an acceptable level of spurious currents. Moreover, these relations are of paramount importance in the design of new experiment dedicated to this topic.

In further calculations, the main point will be to exhibit a critical Bejan number Be_C which characterizes the critical pressure gradient that can expel the drop. But Be_C is a function of several other parameters describing the problem. A consequent study will allow determining the range of crack into which some droplets can be stuck and stop the flow, even under high-pressure gradients like in the industrial problem. Moreover, if two or more capillary bridges are present into the crack, the situation may change and the interactions between capillary bridges should be investigated in future studies. Heat transfer caused by vapor condensation along the crack, modifies the shape of the crack by thermal dilatation; this effect should be taken into account in future calculations.

Moreover, the tortuosity is of relevant interest and will be taken into account in future calculations.

Moreover, simulations based on the CO-

PAIN test cases should be performed in future studies in order to determine the air mass fraction and the gas temperature to be imposed at entrance of the crack in future experiments. Indeed, the thickness of the wall is about 20cm in experiments which is much smaller than in industrial applications; as a consequence, the conservation of the pressure gradient along the crack imposes a specific value of the pressure at inlet (outlet pressure is 1bar). Finally, air mass fraction and gas temperature have to be optimized in order to keep a representative level of vapor condensation along the crack.

ACKNOWLEDGMENTS

This work has been achieved in the framework of the CIWAP3 project, ACCIDENTS GRAVES project and MULTIPATH project financially supported by EDF (Electricité de France). The calculations have been performed with NEPTUNE.CFD code which is being developed in the framework of the NEPTUNE project financially supported by EDF (Electricité de France), CEA (Commissariat à l’Energie Atomique et aux Energies Alternatives), IRSN (Institut de Radioprotection et de Sûreté Nucléaire) and FRAM-ATOME.

REFERENCES

- [Bonometti and Magnaudet, 2006] Bonometti, T. and Magnaudet, J. (2006). An interface-capturing method for incompressible two-phase flows. Validation and application to bubble dynamics. *International Journal of Multiphase Flow*.
- [Brackbill et al., 1992] Brackbill, J., Kothe, D. B., and Zemach, C. (1992). A continuum method for modeling surface tension. *Journal of Computational Physics*.
- [Coquerelle and Glockner, 2015] Coquerelle, M. and Glockner, S. (2015). A fourth-order accurate curvature computation in a level set framework for two-phase

- flows subjected to surface tension forces. *Journal of Computational Physics*.
- [Fleau, 2017] Fleau, S. (2017). *Multifield approach and interface locating method for two-phase flows in nuclear power plant*. PhD thesis, Université Paris-Est.
- [Francois et al., 2006] Francois, M., Cummins, S., Dendy, E., Kothe, D., Sicilian, J., and Williams, M. (2006). A balanced-force algorithm for continuous and sharp interfacial surface tension models within a volume tracking framework. *Journal of Computational Physics*.
- [Fujimoto et al., 2007] Fujimoto, H., Shiotani, Y., and Tong, A. (2007). Three-dimensional numerical analysis of the deformation behavior of droplets impinging onto a solid substrate. *International Journal of Multiphase Flow*.
- [Guillaument et al., 2014] Guillaument, R., Vincent, S., and Caltagirone, J.-P. (2014). An original algorithm for VOF based method to handle wetting effect in multiphase flow simulation. *Mechanics Research Communications*.
- [Ishii, 1975] Ishii, M. (1975). *Thermo-fluid dynamic theory of two-phase*. Eyrolles, University of Michigan.
- [Malet et al., 2014] Malet, J., Parduba, Z., Mimouni, S., and Travis, J. (2014). Achievements of spray activities in nuclear reactor containments since the last decade. *Annals of Nuclear Energy*, 74.
- [Mimouni et al., 2017a] Mimouni, S., Benguigui, W., Fleau, S., Foissac, A., Guingo, M., Hassanaly, M., Laviéville, J., Malet, J., Méchitoua, N., Mérioux, N., and Vincent, S. (2017a). Dispersed Two-Phase Flow Modelling for Nuclear Safety in the NEPTUNE.CFD Code. *Science and Technology of Nuclear Installations*, 2017.
- [Mimouni et al., 2017b] Mimouni, S., Fleau, S., and Vincent, S. (2017b). CFD calculations of flow pattern maps and LES of multiphase flows. *Nuclear Engineering and Design*, 321.
- [Mimouni et al., 2011a] Mimouni, S., Foissac, A., and Laviéville, J. (2011a). CFD modelling of wall steam condensation by a two-phase flow approach. *Nuclear Engineering and Design*, 241(11):4445–4455.
- [Mimouni et al., 2010] Mimouni, S., Lamy, J.-S., Laviéville, J., Guieu, S., and Martin, M. (2010). Modelling of spray containment applications with a CMFD code. *Nuclear Engineering and Design*, 240(9):2260–2270.
- [Mimouni et al., 2011b] Mimouni, S., Méchitoua, N., and Ouraou, M. (2011b). CFD Recombiner Modelling and Validation on the H_2 -Par and Kali- H_2 Experiments. *Science and Technology of Nuclear Installations*, 2011.
- [Méchitoua et al., 2012] Méchitoua, N., Mimouni, S., Ouraou, M., and Moreau, E. (2012). CFD MODELLING OF THE TEST 25 OF THE PANDA EXPERIMENT.
- [Persoff et al., 1995] Persoff, P., Pruess, K., and Myer, L. (1995). Two-phase flow visualisation and relative permeability measurement in Transparent Replicas of rough-walled rock fractures. *Water Resources Research*.
- [Popinet and Zaleski, 1999] Popinet, S. and Zaleski, S. (1999). A Front-tracking algorithm for accurate representation of surface tension. *International Journal of Numerical Methods in Fluids*.
- [Quéré, 1997] Quéré, D. (1997). Inertial capillarity. *Europhysics letters*.

- [Rastiello et al., 2015] Rastiello, G., Leclaire, S., Belarbi, R., and Benacer, R. (2015). Unstable two-phase flow rate in micro-channels and cracks under imposed pressure difference. *International Journal of Multiphase Flow*.
- [Renardy and Renardy, 2002] Renardy, Y. and Renardy, M. (2002). PROST : A Parabolic Reconstruction of Surface Tension for the Volume-of-Fluid Method. *Journal of Computational Physics*.
- [Turner et al., 2004] Turner, S., Lam, L., Faghri, M., and Gregory, O. (2004). Experimental investigation of gas flow in microchannels. *Journal of Heat Transfert*.
- [Vincent et al., 2016] Vincent, S., Tavares, M., Fleau, S., Mimouni, S., Ould-Rouiss, M., and Estivalezes, J.-L. (2016). A priori filtering and LES modeling of turbulent two-phase flows. Application to phase separation. *Computers and Fluids*, 000.
- [Wang et al., 2014] Wang, M.-J., Hung, Y.-L., Lin, F.-H., and Lin, S.-Y. (2014). Dynamic behaviors of droplet impact and spreading : A universal relationship study of dimensionless wetting diameter and droplet height. *Experimental Thermal and Fluid Science*.
- [Washburn, 1921] Washburn, E. W. (1921). The dynamic of capillary flow. *The Physical Review*.